Politecnico di Torino

ENERGY CENTER

unite! University Network for Innovation, Technology and Engineering

CSP COUPLED TO POLYGENERATION SYSTEMS – CASE STUDY: ENERGY CENTER ROOFTOP

Davide Papurello

Unite! CSP-IMT
Concentrated Solar Power and Solar cells - Innovative Materials and Technologies (CSP-IMT) sustainable electricity and heat generation – Training and Innovation –
ONLINE 02/07/2026

INDEX:

- Solar concentrators (parabolic dish conc.)
- Uses of the solar concentrator:
  - Stirling engine
  - ORC cycle
  - Chemical looping

Politecnico di Torino
ENERGY CENTER
unite! University Network for Innovation, Technology and Engineering

TYPES OF HIGH-TEMPERATURE CONCENTRATED SOLAR PANELS (CSP)

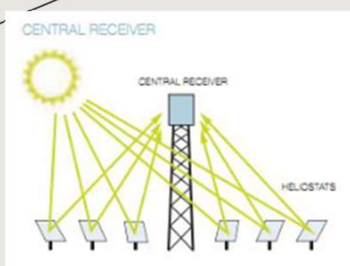

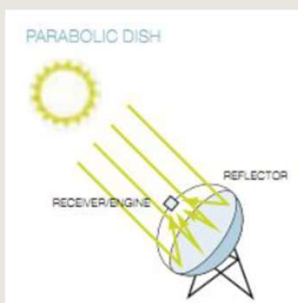

Types	Concent.	ε_{MAX} [%]	T_{MAX}[°C]	Sizes
Linear parabolics	70-80	40-50	600	100 m * 6 m
Solar towers	500-1000	60-68	1200	50-150 m^2
Parabolic discs	300-2000	60-70	1400	6-10 m (diameter)

M. Falchetta T. Crescenzi, 2016 (https://www.pubblicazioni.enea.it/le-pubblicazioni-enea/edizioni-enea/anno-2016/opportunita-di-applicazione-delle-tecnologie-solari-termodinamiche-in-italia.html).

Politecnico di Torino
ENERGY CENTER

unite! University Network for Innovation, Technology and Engineering

PARABOLIC DISH CONCENTRATOR

PARABOLIC DISH CONCENTRATOR

Experimental tests were conducted using a solar concentrator under real conditions at the Energy Center of Turin, Politecnico di Torino, Italy (45.0676 N, 7.6563 E). The concentrator consists of a single solar dish with an aperture of approximately 2.4 m. The system is equipped with two motors able to control the azimuth and the elevation of the dish to follow the Sun's movements in the sky.

Symbol	Description	Value	U.m.
D_c	Diameter of the dish	2370	mm
f	Focal distance	958	mm
y_R	Depth	370	mm
φ_R	Rim angle	61.89	°
Co	Optical Concentration ratio	8013	-
d_f	Diameter of the focal point	6.41	mm
l	Length of the receiver	200	mm
A	Area of the concentrator	4.5	m^2
P	Power of the concentrator	2.8	kW

PARABOLIC DISH CONCENTRATOR

unite! University Network for Innovation, Technology and Engineering

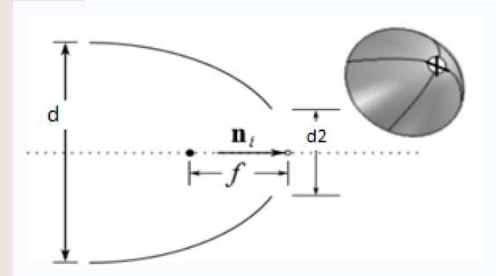

Increasing focal length f and constant edge angle φ

$$d = 4 \cdot f \cdot [\csc(\varphi) - \cot(\varphi)] \rightarrow D_{focal\ plane} = \frac{d\,\dfrac{\sin\theta_s}{\sin\varphi}}{\cos\varphi}$$

$$A_{opening} = \frac{\pi \cdot d^2}{4} \rightarrow P = I_0 \cdot A$$

Source power

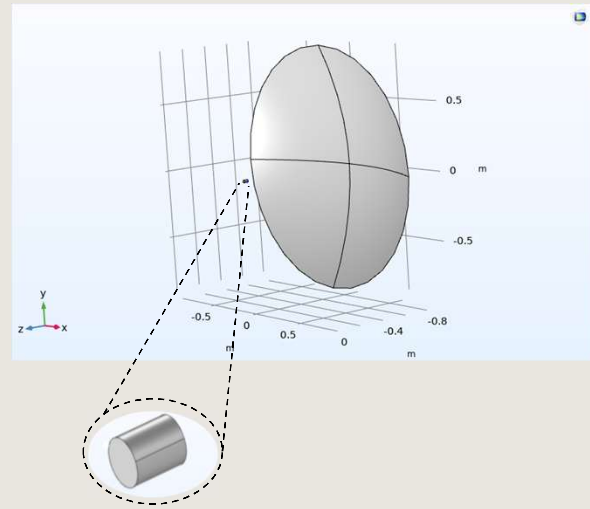

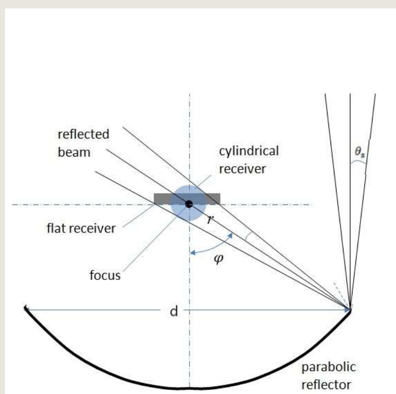

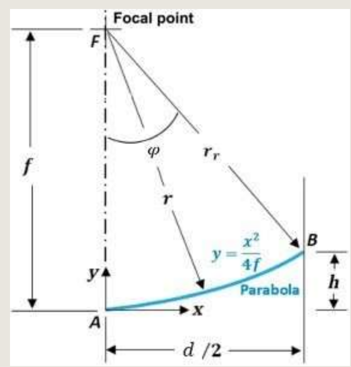

K. Lovegrove and J. Pye, "Fundamental principles of concentrating solar power systems," in Concentrating Solar Power Technology, Elsevier, 2021.

PARABOLIC DISH CONCENTRATOR

- Not all incident rays are parallel because a finite source size is imposed. They are sampled by a narrow cone with a maximum angle equal to the solar acceptance angle θ_s.
- Part of the incoming radiation is absorbed by the surface of the concentrator. Only part of the incident radiation is reflected back to the receiver.
- The phenomenon of 'edge dimming' is an optical effect seen in stars where the central part of the disc appears brighter than the edge. It is responsible for the decrease in the intensity of solar radiation emitted from the centre to the vicinity of the visible disc.
- The last dissipative effect concerns the roughness of the collector surface. Concentrators that are mirrors have local ripples and distortions in their surfaces. Not having a perfectly smooth surface leads to deflections of the reflected rays from the surface itself resulting in an increase in the area over which the radiation is reflected along the focal plane. This effect is called surface slope error.

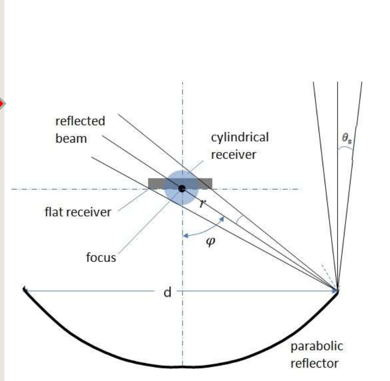

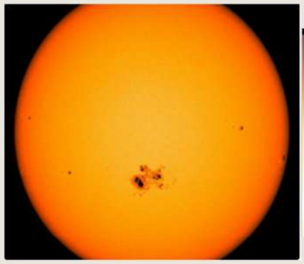

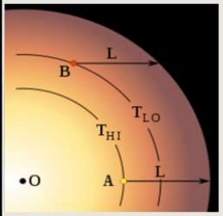

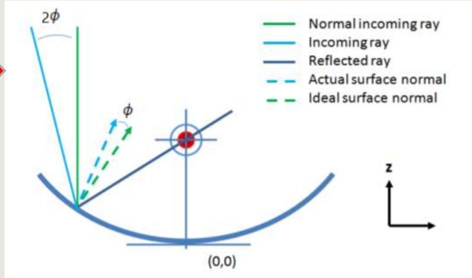

PARABOLIC DISH CONCENTRATOR

$C = \frac{I}{I_0}$ Local optical concentration ratio

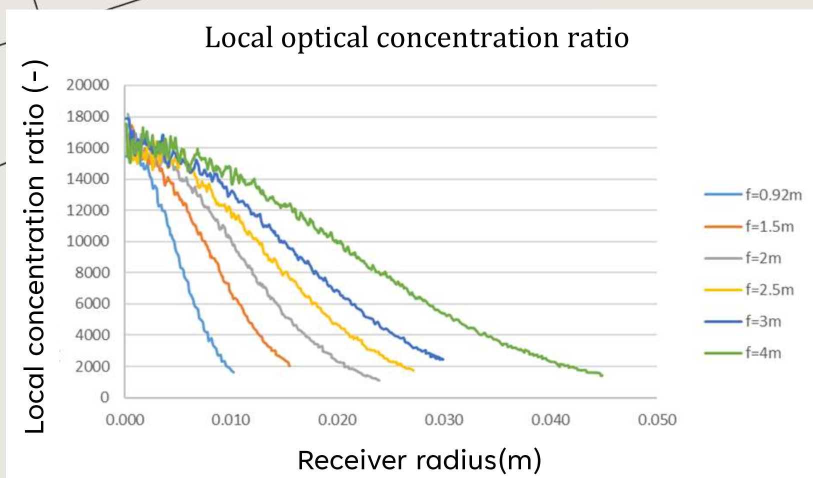

Ideal reflection

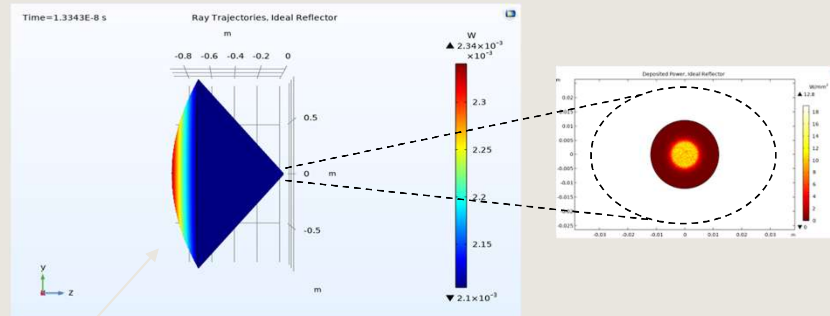

Real reflection

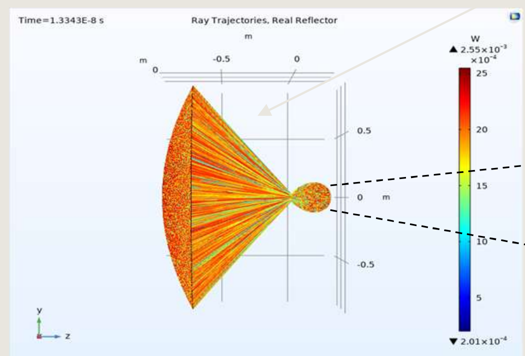

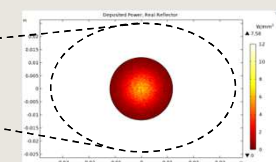

PARABOLIC DISH CONCENTRATOR

Receiver losses

$$\dot{Q}_{\text{rad}} = \varepsilon \sigma A T^4 \quad \rightarrow \quad \dot{Q}_{\text{rad}} = \varepsilon \sigma A (T_{\text{rec}}^4 - T_{\text{amb}}^4)$$

Radiative losses

$$\dot{Q}_{\text{conv}} = hA(T_{\text{rec}} - T_{\text{amb}})$$

Convection Losses

h [W/m2·K], is calculated by empirical correlations and depending on the property of the fluid (such as viscosity, density, and thermal conductivity), the flow regime and direction, the surface geometry.

$$h = \frac{k}{D}\left(0.3 + \frac{0.62 \cdot \text{Re}_D^{1/2} \cdot \text{Pr}^{1/3}}{\left(1 + \left(\frac{0.4}{\text{Pr}}\right)^{2/3}\right)^{1/4}}\left(1 + \left(\left(\frac{\text{Re}_D}{282000}\right)^{5/8}\right)^{4/5}\right)\right)$$

$$\dot{Q}_{\text{cond}} = kA\frac{(T_{\text{rec}} - T_{\text{amb}})}{L}$$

Conduction Losses

Total Losses

$$\dot{Q}_{\text{loss}} = \dot{Q}_{\text{rad}} + \dot{Q}_{\text{conv}} + \dot{Q}_{\text{cond}}$$

$$\dot{Q}_{\text{input}} = I_{\text{in}} \cdot C_r \cdot A_{\text{ap}}$$

$$\eta_{\text{rec}} = \frac{\dot{Q}_{\text{converted}}}{\dot{Q}_{\text{input}}} = \frac{\dot{Q}_{\text{input}} - \dot{Q}_{\text{tot loss}}}{\dot{Q}_{\text{input}}}$$

PARABOLIC DISH CONCENTRATOR

- The receiver is a black body so the temperature is calculated using the Stefan-Boltzmann law.
- $I_{receiver}$ is the destruction of solar radiation concentrated on the receiver area.

$$T = \sqrt[4]{\frac{I_{receiver}}{\sigma}}$$

- The maximum temperature that can be reached at the centre of the receiver increases with focal length as the more power is deposited locally.

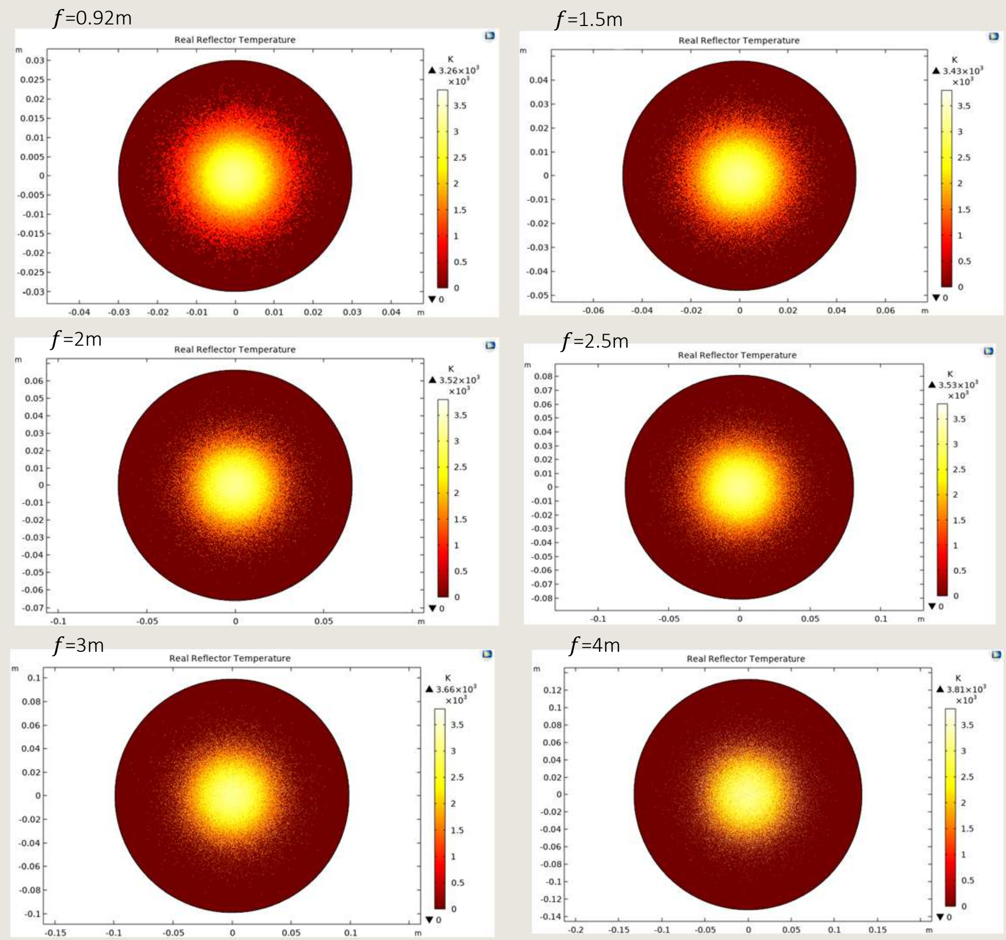

Politecnico di Torino
ENERGY CENTER

unite! University Network for Innovation, Technology and Engineering

STIRLING ENGINE

STIRLING ENGINE

- External combustion engine
- The hot-side heat exchanger radiated by the external heat source
- The regenerator is used to improve engine performance: decrease expansion and compression work
- 2 configurations: single-cylinder (ML1000) and twin-cylinder (ML3000)

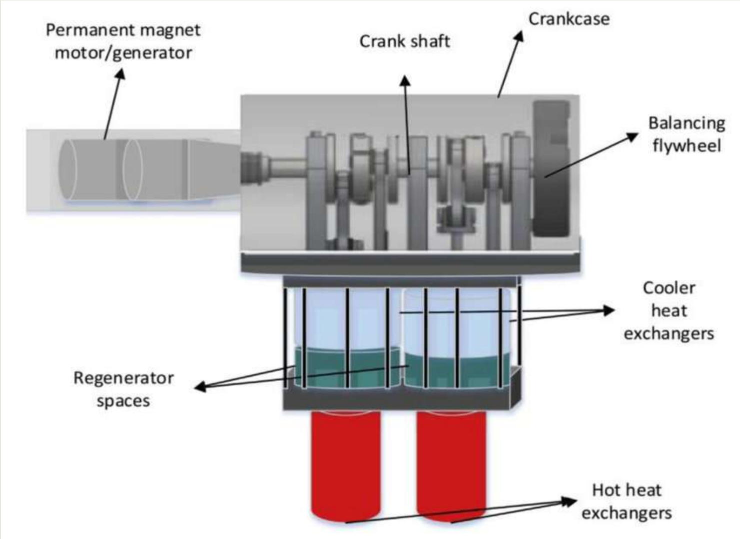

STIRLING ENGINE

PARAMETERS	VALUE	UNITS OF MEASUREMENT
Geometric Parameters		
Connecting rod length	210	mm
Cylinder diameter	110	mm
Piston stroke	55.2	mm
Compression/expansion cycle phase shift	90	°
Volume (displacement) compression cylinder	524.6	cm^3
Volume (displacement) expansion cylinder	524.6	cm^3
"Dead" space compression cylinder	153.3	cm^3
Space "dead" expansion cylinder	153.3	cm^3
Operating Parameters		
Rotational speed	600	rpm
Working fluid	air	-
Average pressure indicated	15	bar
Coolant	water	-
Warm Side Starting Temperature	700	°C

ENGINE FEATURES

STIRLING ENGINE

HOT-SIDE EXCHANGER DESIGN

EXCHANGER FEATURES	
Number of tubes	9
Outer diameter (mm)	20
Inner diameter (mm)	14
Tube thickness (mm)	3
Maximum Tube Height (mm)	120
Distance between twin-cylinder engine centers (mm)	274

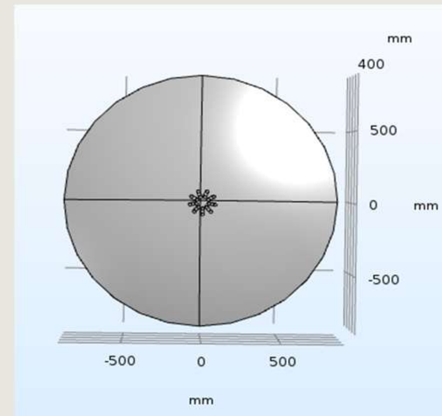

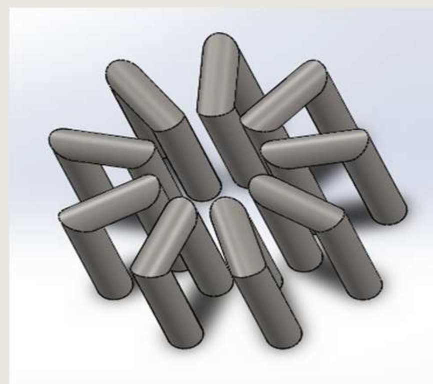

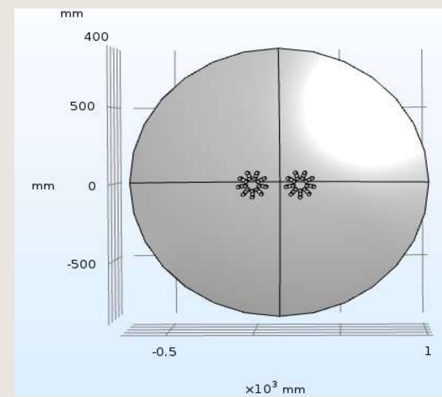

STIRLING ENGINE

OPERATING PARAMETERS

- Concentrator diameter : 1,78 m
- Irradiation : 800 W/m^2
- Focal length : 0,92 m
- Sampling angle of the conical distribution: 4,65 mrad
- Surface roughness : 1,75 mrad

Stefan-Boltzmann law

$$T = \left(\frac{q}{\sigma}\right)^{0,25}$$

q: boundary heat source (W/m^2)

σ: Stefan-Boltzmann constant

$\sigma = 5.67 \cdot 10^{8}$ W/(m^{2}K^4)

Physical properties	AISI 310	Inconel 625
Density (kg/m^3)	7550	8440
Thermal capacity at constant pressure (J/kg/K)	610	560
Thermal conductivity (W/m/K)	23.7	20.3

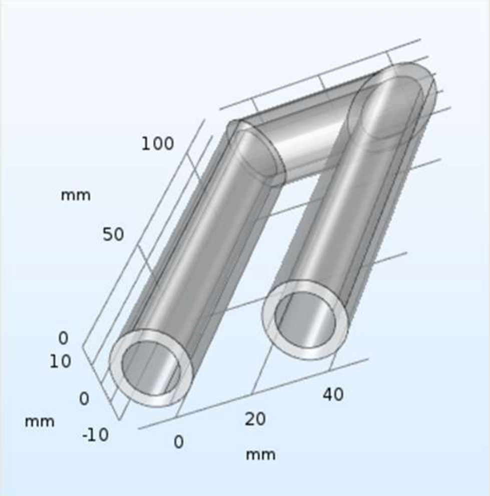

STIRLING ENGINE

REAL STIRLING CYCLE

FIRST ORDER method: Beale's equation

$$P = Be \cdot p \cdot f \cdot V_0$$

- P: heat output (W)
- p: average pressure in the cycle (bar)
- f: cycle frequency (Hz)
- V_0: engine piston displacement (cm^3)
- Be: number of Beale

Number of Beale	-	0.015
Average pressure in the cycle	bar	15
Cycle frequency	Hz	10
Piston displacement	cm^3	524.6
Thermal power	**W**	**3780**

EQUATION FOR TWO-PISTON ENGINES

$$W = P \cdot V_T \cdot \frac{\pi \cdot (1 - AU)}{K + 1} \cdot \left(\frac{1 - DL}{1 + DL}\right)^{1/2} \cdot \frac{DL \cdot \sin(ET)}{1 + (1 - DL^2)^{1/2}}$$

G. Walker, «Stirling Engines», Oxford University Press, 1980

- p: maximum pressure in the cycle (MPa)
- V_T: total swept volume, sum of cold and hot side : V_T = VL+VK (cm^3)
- VL: swept volume in the expansion phase (cm^3)
- VK: volume swept in the compression phase (cm^3)
- K: swept volume ratio : K = VK/VL
- AU: ratio of cold-side to hot-side temperatures
- TC: temperature on the cold side measured in K
- TH: measured hot-side temperature in K
- TR: regenerator temperature (K)
- AL: phase angle measured in degrees, equal to 90° in alpha-Stirling engines
- VD: total sum of dead volumes (cm^3)
- RV: “dead volume ratio”, VD/VL

STIRLING ENGINE

Definition	Symbol	Units of measurement	Value
Maximum pressure in the cycle	P	MPa	2.1
Total swept volume	VT	cm^3	1049,2
Expanding swept volume	VL	cm^3	657,94
Volume swept in compression	VK	cm^3	569,05
Swept volume ratio	K	-	1,16
Cold side temperature	TC	K	313
Hot-side temperature	TH	K	1132
Temperature ratio	AU	-	0,28
Regenerator temperature	TR	K	637,09
Phase angle	AL	°	90
Total dead volume	VD	cm^3	459,9
Dead volume ratio	RV	-	0,70
Calculation of Walker's parameters			
	S	-	0,30
	DL	-	0,58
	ET	°	76,55
Work per engine cycle	W	J/cycle	372.98
Thermal power	P_{th}	W	3729.8
Yield	%	-	30
Effective power	$\mathbf{P_{eff}}$	**W**	**1118.93**

$$S = \frac{2 \cdot RV \cdot AU}{AU + 1}$$

$$DL = \frac{(AU^2 + 2 \cdot AU \cdot K \cdot \cos(AL) + K^2)^{1/2}}{(AU + K + 2 \cdot S)}$$

$$ET = tan^{-1}\left(\frac{K \cdot \sin(AL)}{AU + K \cdot \cos(AL)}\right)$$

STIRLING ENGINE

Parameter	Units of Measure	Value
Average irradiation on the concentrator	W/m^2	800
Hot side fluid temperature	°C	859
Thermal power	kW	1.12
Electric generator efficiency	%	88
Electric power generated	kW	0.99

ORC CYCLE

ORC CYCLE

1–2 : Adiabatic compression of the liquid, not a reversible transformation since the increase in entropy is accounted for by the pump efficiency η_p

2–2' : Heating at constant pressure of the fluid until the saturation temperature

2'–3 : Vaporization at constant pressure until the state of superheated saturated vapor

3–4 : Irreversible adiabatic expansion, with a loss evaluated by the turbine efficiency η_t

4–1 : Heat removal at constant pressure until returning to the initial condition of saturated liquid

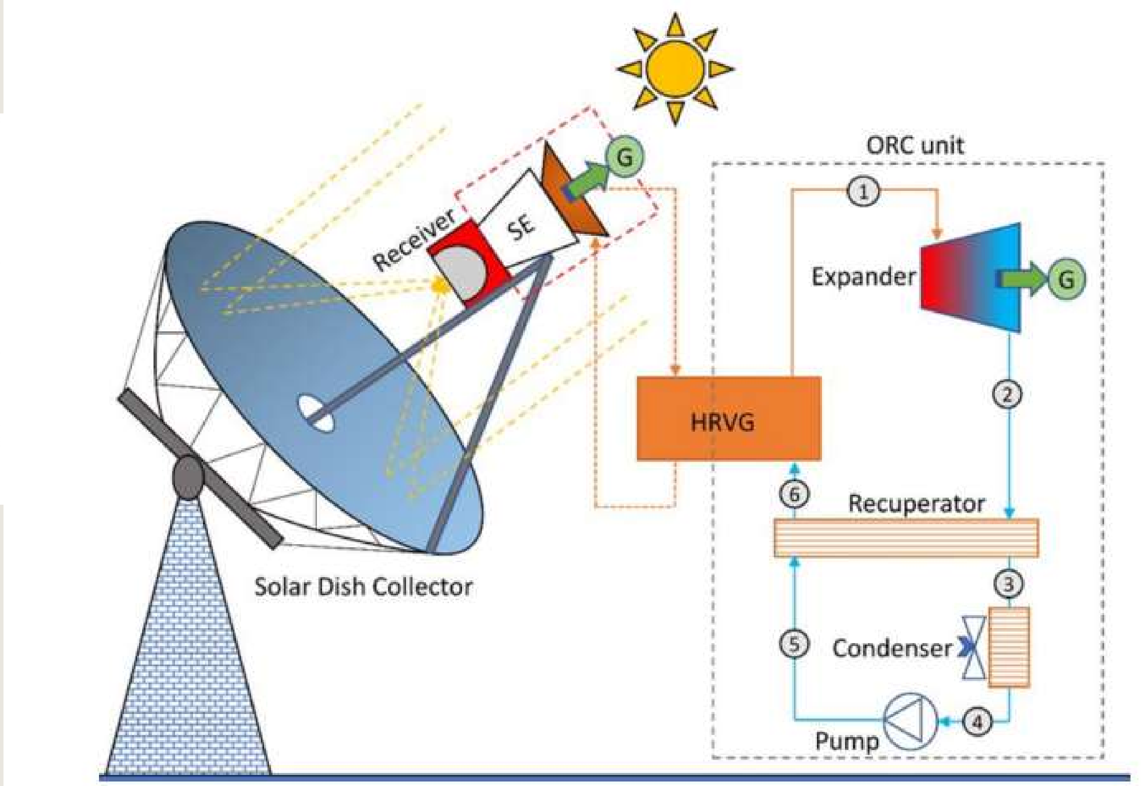

10.1051/e3sconf/202131306001

ORC CYCLE

Working Fluids

Acetone

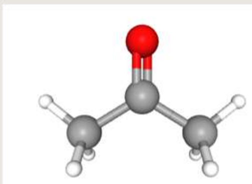

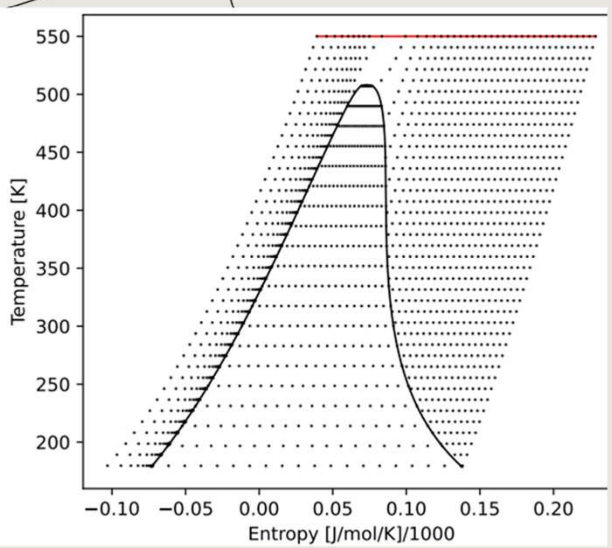

MD2M

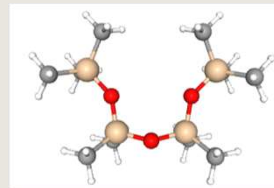

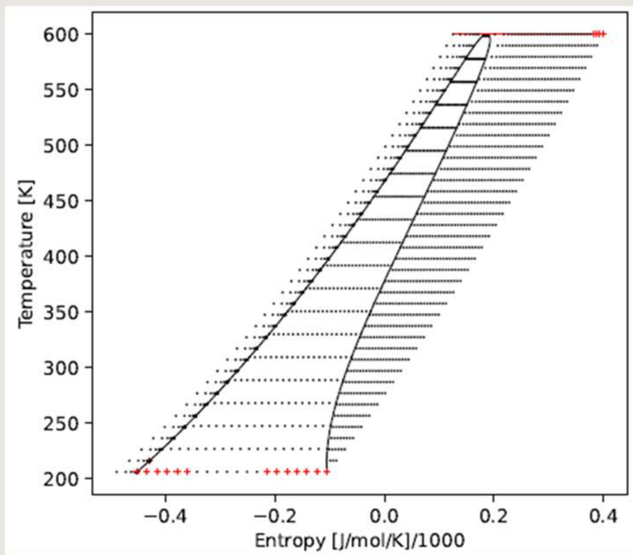

n-Butane

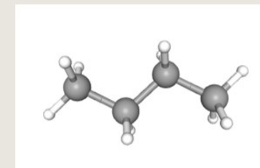

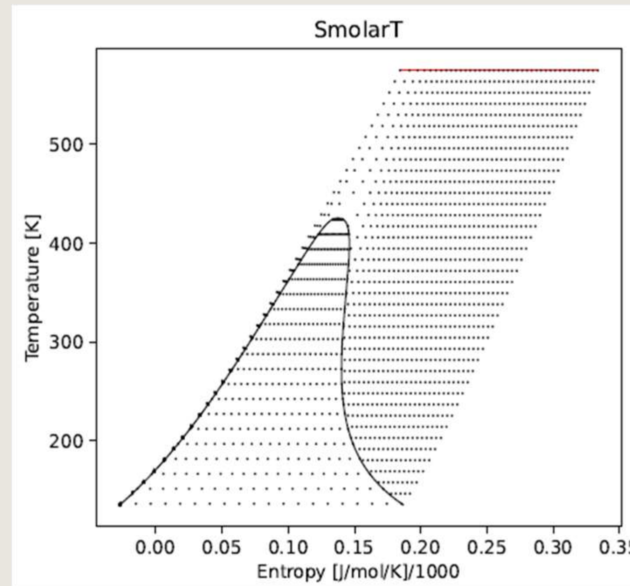

ORC CYCLE

ORC with Acetone

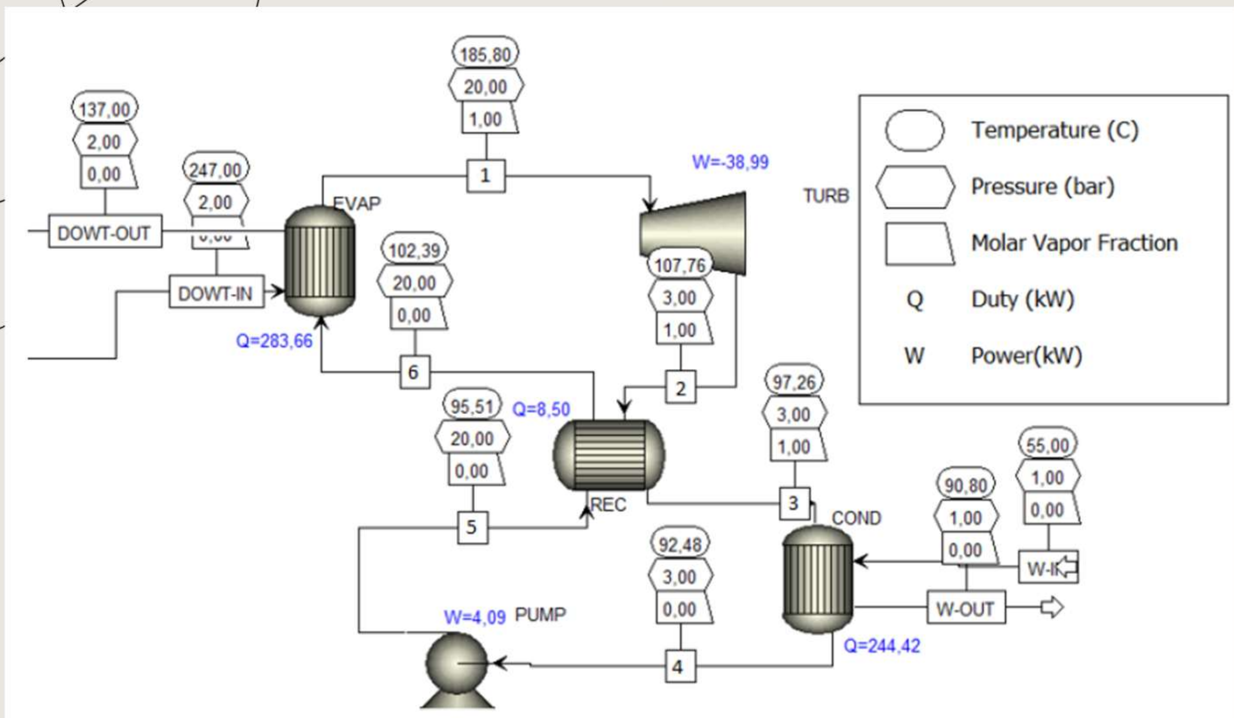

	Aver.	Max	Min
Pel [kWel]	20	47	6
Qcond [kWth]	220	252	240
Tdow [°C]	290	400	210

ORC CYCLE

ORC with Butane

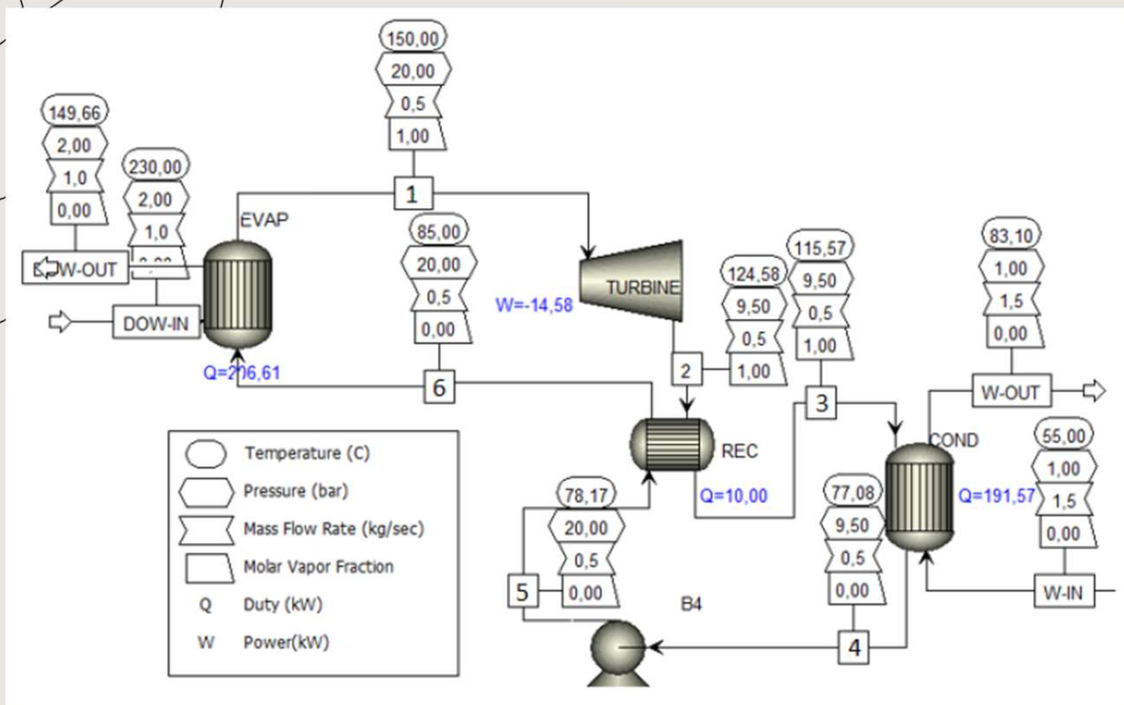

	Med	Max	Min
Pel [kWel]	13	15	6
Qcond [kWth]	172	176	152
Tdow [°C]	190	220	160

ORC CYCLE

ORC with MD2M

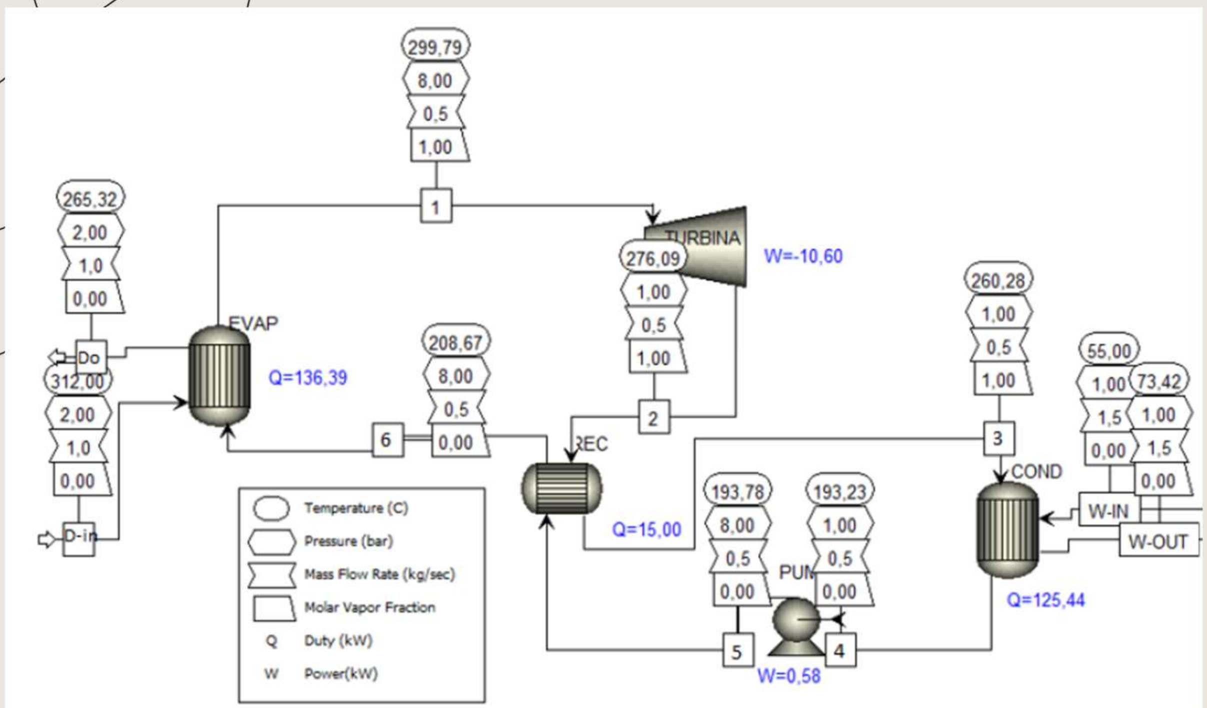

	Med
Pel [kWel]	10
Qcond [kWth]	125
Tdow [°C]	312

ORC CYCLE

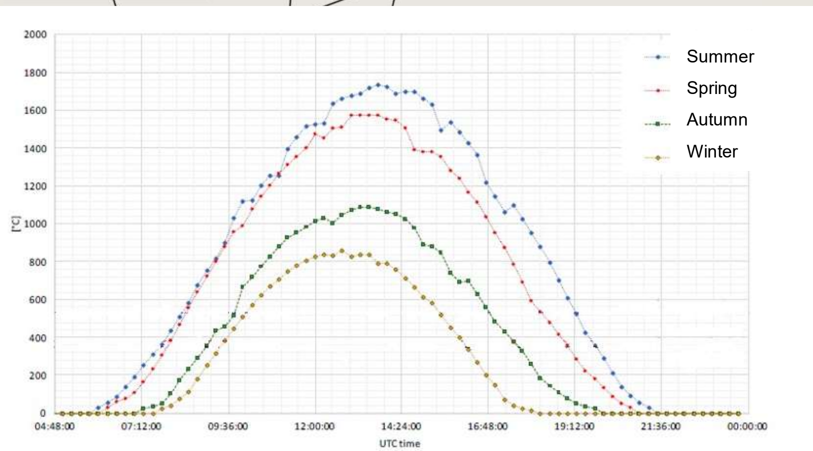

Small parabolic dish solar concentrator with a reflecting surface of 4.5 m^2 located at the Energy Centre

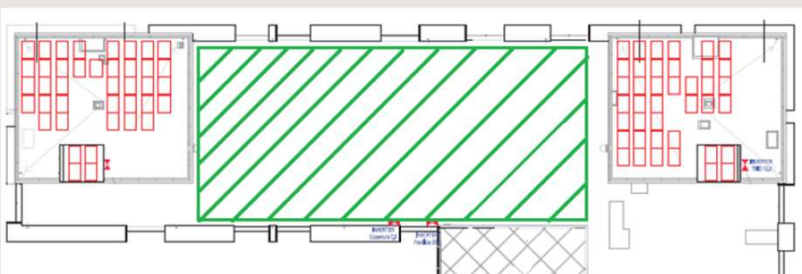

Available area: 580 m^2

Installable concentrators: 14

Real Operation

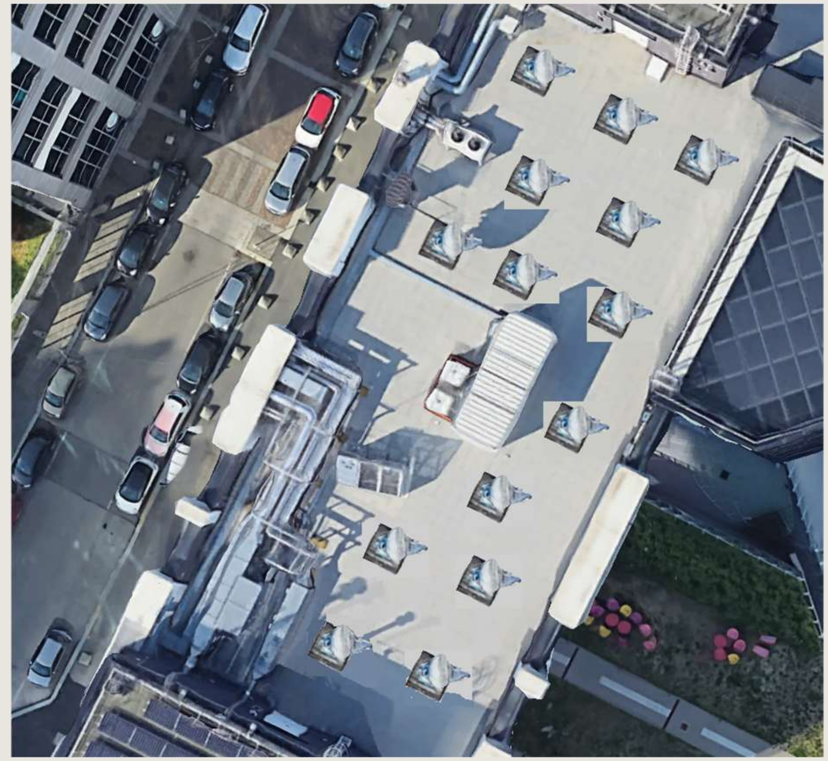

	Acetone	MD2M	n-Butane
Power produced by a disc collector (kW)	2,67	2,64	2,6

Politecnico di Torino
ENERGY CENTER

unite! University Network for Innovation, Technology and Engineering

CHEMICAL LOOPING USING A SOLAR CONCENTRATOR

PRELIMINARY WORK ON THE CHEMICAL LOOPING USING A SOLAR CONCENTRATOR

Solar Power

Methane
(eventually)

Chemical Looping
by making use of iron oxides

Concentrating solar power facility
on the Energy Center rooftop

Hydrogen or a syngas

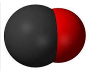

PRELIMINARY WORK ON THE CHEMICAL LOOPING USING A SOLAR CONCENTRATOR

Reduction Reaction

Suitable range of temperature for pure reduction is between 1400-1600° C https://doi.org/10.1016/j.solener.2017.05.032

Complete reaction from Fe3O4 to FeO has zero Gibbs free energy around 2400 °C in air https://doi.org/10.1016/j.ijhydene.2004.02.019

By adding methane to the reducing atmosphere it is possible to lower the temperature range: 600-1000°C https://doi.org/10.1016/j.cherd.2010.12.017

Chemical Looping Combustion (CLC)

Methane Chemical Looping Reforming (MCLR)

Chemical Looping Partial Oxidation (CLPO)

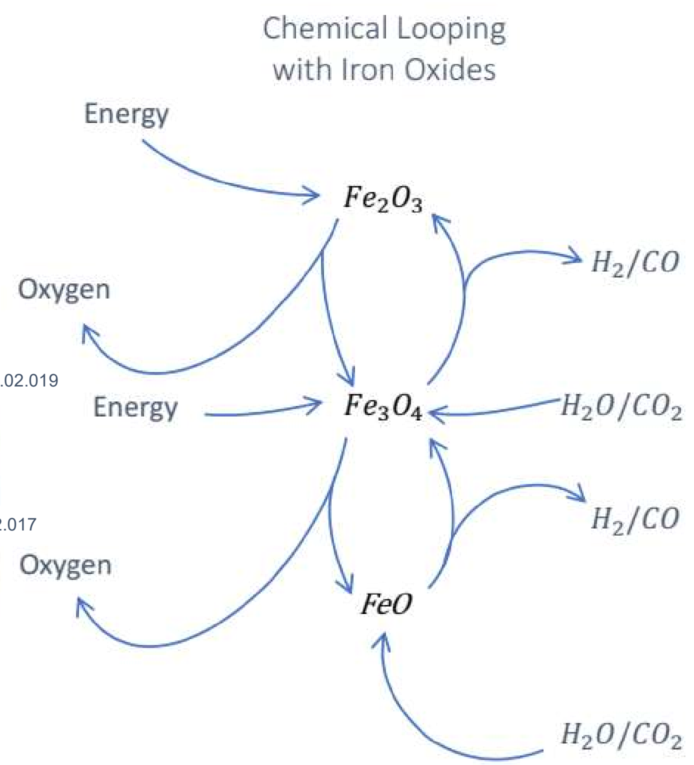

PRELIMINARY WORK ON THE CHEMICAL LOOPING USING A SOLAR CONCENTRATOR

Solar Concentrator

Test Bench in real conditions

Dish diameter:	D_c	2370 mm
Depth of the dish:	y_R	370 mm
Dish Area:	A	4.5 m [2]
Power:	P	2.8 kW [2]

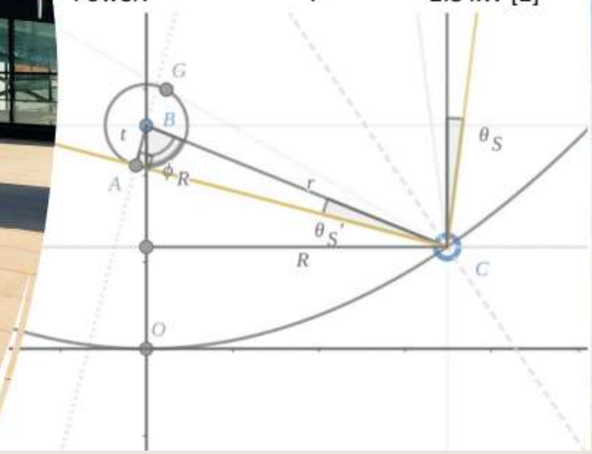

PRELIMINARY WORK ON THE CHEMICAL LOOPING USING A SOLAR CONCENTRATOR

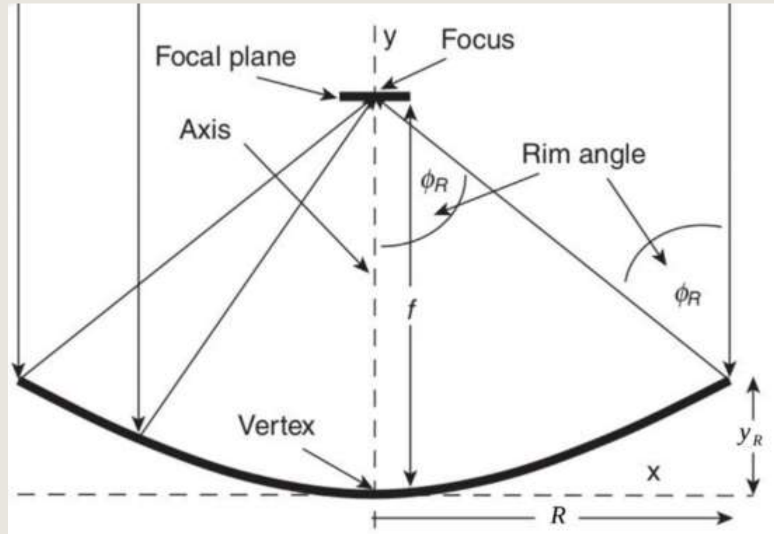

OVERVIEW

This work investigates methane-assisted chemical looping (MCLC/CLR) with iron oxides in a solar concentrator. Experiments were performed in a solar reactor to produce syngas (H_2 + CO) at high temperature (>1000 K). Experimental results were compared with multiphysics simulations for validation of the thermal field and chemical behavior

PRELIMINARY WORK ON THE CHEMICAL LOOPING USING A SOLAR CONCENTRATOR

Solar Concentrator: measured temperatures

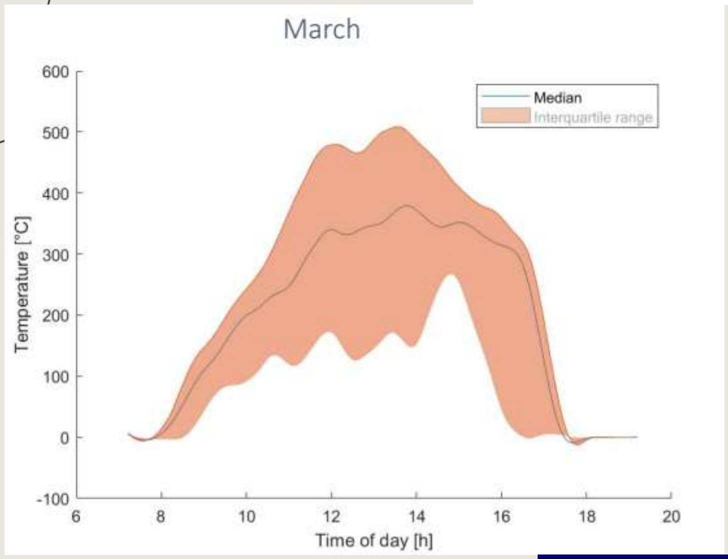

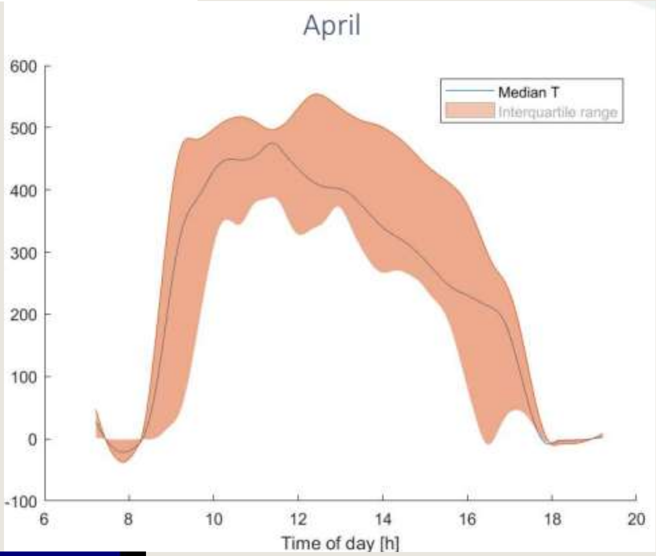

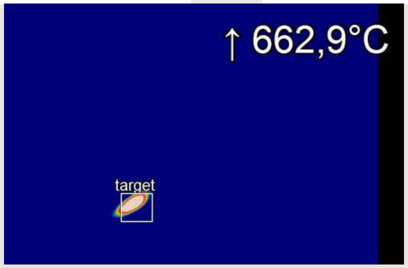

PRELIMINARY WORK ON THE CHEMICAL LOOPING USING A SOLAR CONCENTRATOR

Experimental Tests: #3, #4, #5

Solar Concentrator and Reactor
A solar tower facility with a heliostat field concentrates solar flux onto a tubular receiver.

Reactor Configuration
Cylindrical fixed-bed reactor (quartz window at the top), exposed to concentrated solar radiation.

Oxygen Carrier
Hematite (α-Fe_2O_3) particles (125–250 µm) are used as oxygen carrier.

Gas Analysis
The outlet gas is analyzed by online GC to determine H_2, CO, CO_2 and CH_4 concentrations.

Numerical Modelling (COMSOL Multiphysics®)
A coupled model (heat transfer + chemistry + fluid flow) is developed to simulate the reactor and predict gas composition and temperatures.

Model geometry and domains (from Fig. 1)

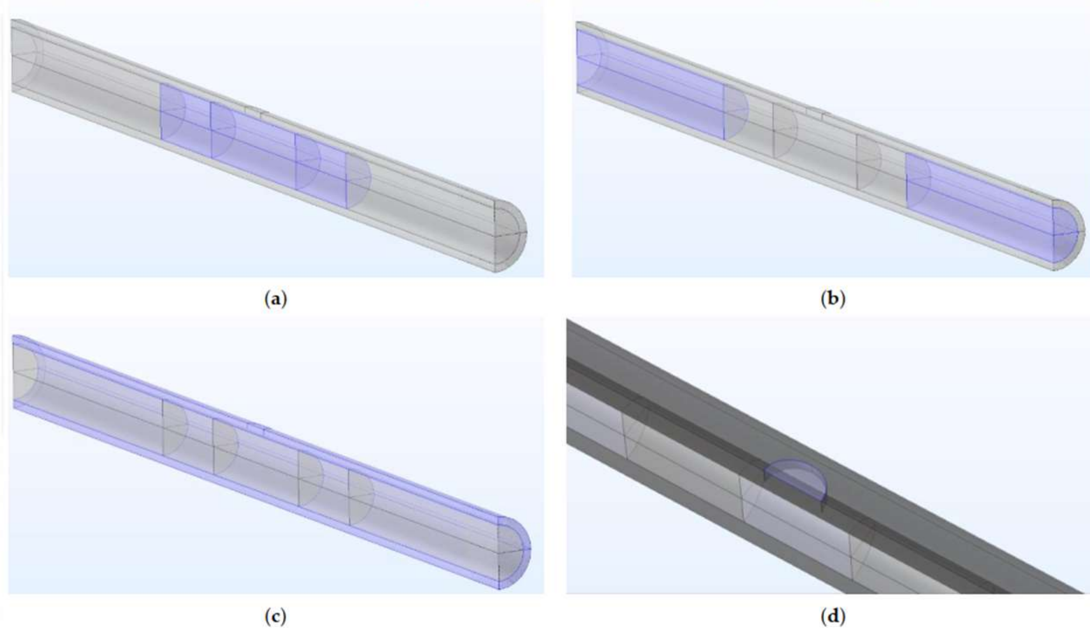

Figure 1. **(a)** Porous domain. **(b)** Fluid domain. **(c)** Solid domain. **(d)** Area exposed to the heat solar flux.

The reactor is vertically oriented and directly irradiated by concentrated solar flux. Methane is injected at the bottom.

Borghero et al., (2022)

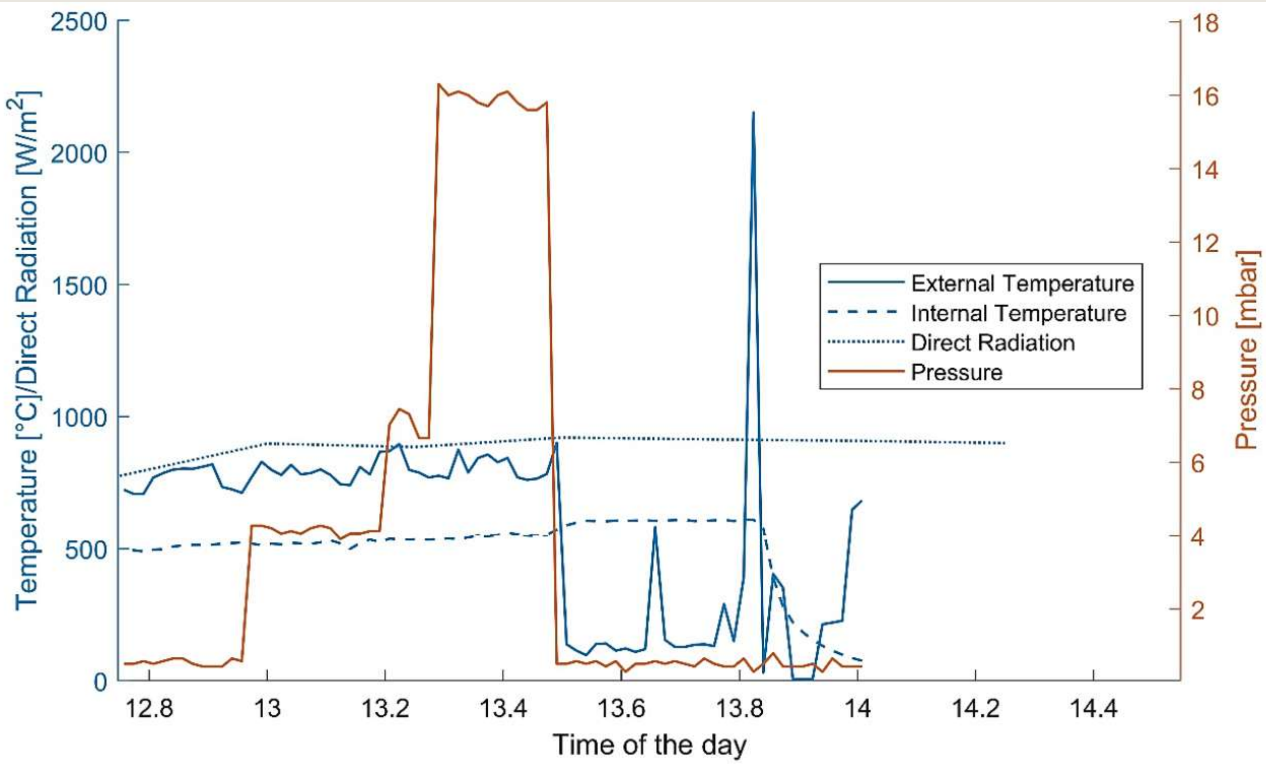

Figure 2 demonstrates that the solar concentrator successfully supplied sufficient thermal energy to initiate methane-assisted reduction of hematite. It also highlights the principal engineering challenge of the process: although the solar reactor achieved the temperatures required for chemical looping, the receiver materials were unable to withstand the severe thermal gradients and localized heat fluxes. This confirms that **material durability and receiver design** are critical factors for the practical implementation of high-temperature solar chemical looping systems

Politecnico di Torino
ENERGY CENTER

unite! University Network for Innovation, Technology and Engineering

Temperature evolution

- Before methane injection, the reactor is heated exclusively by concentrated solar radiation.
- The **external wall temperature** stabilizes around **750–850 °C**, while the **internal temperature** gradually increases to approximately **500–600 °C**.
- According to the validated thermal simulations, the powder bed reaches significantly higher temperatures than those measured by the thermocouples, allowing the reduction reactions to occur.

Solar radiation

- The **direct normal irradiation (DNI)** remains nearly constant throughout the experiment, close to **900 W m^{-2}**, indicating stable weather conditions and continuous solar input.
- This stable irradiation ensures that the observed thermal variations are mainly related to the reaction and material behavior rather than fluctuations in solar intensity.

Methane injection and pressure increase

- At approximately **13.2 h**, the reactor is fed with the **35% CH_4 / 65% N_2** mixture.
- This is evidenced by the rapid increase in reactor pressure from approximately **1 mbar** to **16 mbar**, marking the beginning of the reduction process.

Thermal degradation of the receiver

- Shortly after methane injection, large oscillations appear in the external temperature signal, including a sharp spike above **2000 °C** followed by a sudden collapse.
- These abnormal temperature fluctuations are attributed to **receiver degradation and probable thermocouple damage**, caused by the extremely high thermal stresses generated by concentrated solar flux.
- Eventually, the metallic reactor loses structural integrity, terminating the experiment.

Figure 3 presents the evolution of the outlet gas composition measured during the methane-assisted reduction of hematite in the solar reactor. The concentrations of **H_2, CO, CO_2, CH_4**, and **O_2** are reported together with the reactor pressure as a function of time, allowing the identification of the different reaction stages.

Figure 3. Outlet gas composition (dry basis) and pressure during test #3.

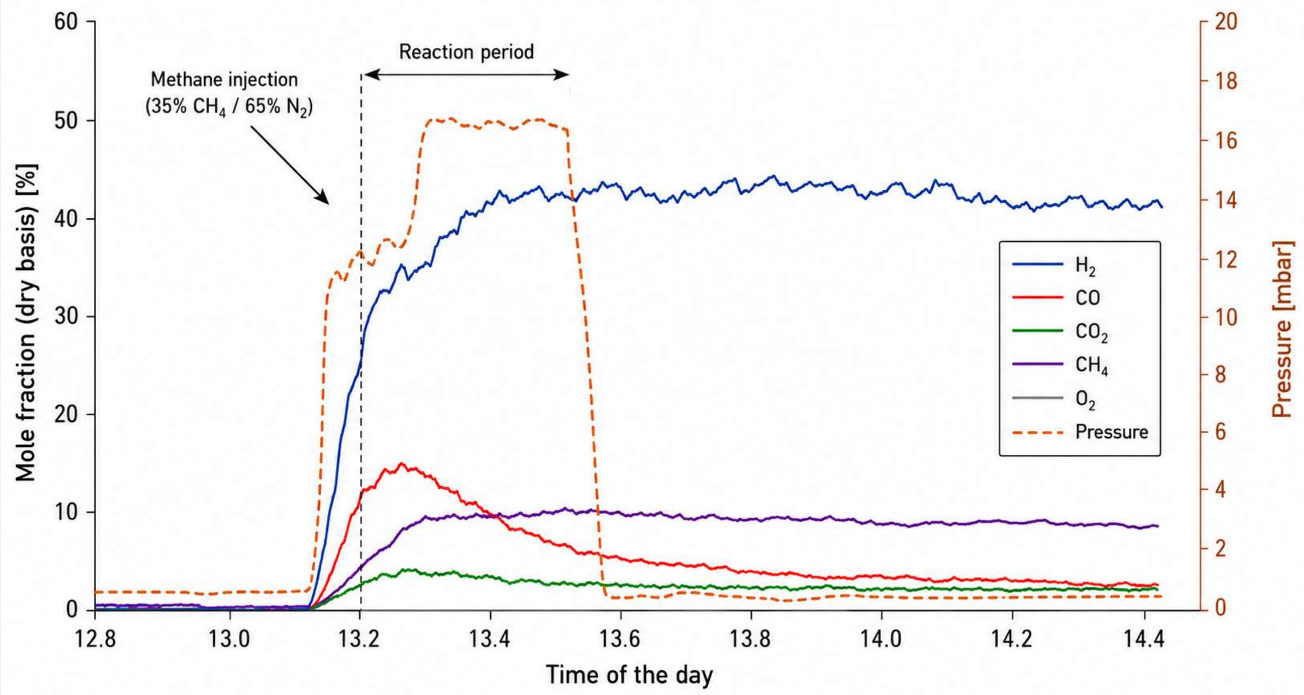

Reaction initiation

- At approximately **13.2 h**, methane is introduced into the reactor, producing an immediate increase in reactor pressure to approximately **16 mbar**.
- Simultaneously, the outlet gas composition changes rapidly, indicating the onset of the reduction reactions.

Hydrogen production

- Hydrogen becomes the dominant product, rapidly reaching concentrations of **40–45%**.
- After the initial increase, the H_2 concentration remains relatively stable during the experiment, demonstrating continuous hydrogen production through methane-assisted reduction and reforming reactions.

Carbon monoxide behavior

- CO exhibits an initial peak of approximately **10–15%**, followed by a gradual decrease as the reduction progresses.
- This behavior suggests that partial oxidation reactions are initially dominant before the oxygen available in the hematite decreases.

Carbon dioxide formation

- CO_2 also shows a short initial peak but remains at considerably lower concentrations than CO.
- The low CO_2 yield indicates that complete methane oxidation is limited, while partial oxidation and reforming reactions are favored under the high-temperature operating conditions.

Residual methane

- A significant amount of **unreacted CH_4** is detected throughout the experiment.
- This indicates incomplete methane conversion, likely caused by imperfect gas-solid contact, cold spots inside the reactor, or kinetic limitations.

Oxygen concentration

- O_2 remains close to zero during the reaction, confirming that oxygen is supplied by the iron oxide lattice rather than by gaseous oxygen.

Figure 3 demonstrates that the solar-driven reactor successfully promotes **chemical looping reforming (CLR)**, producing a hydrogen-rich syngas while limiting complete combustion. The coexistence of H_2, CO, and small amounts of CO_2 confirms that both **chemical looping combustion (CLC)** and **chemical looping partial oxidation (CLPO)** occur simultaneously, with hydrogen production becoming the dominant process.

Figure 3. Outlet gas composition (dry basis) and pressure during test #3.

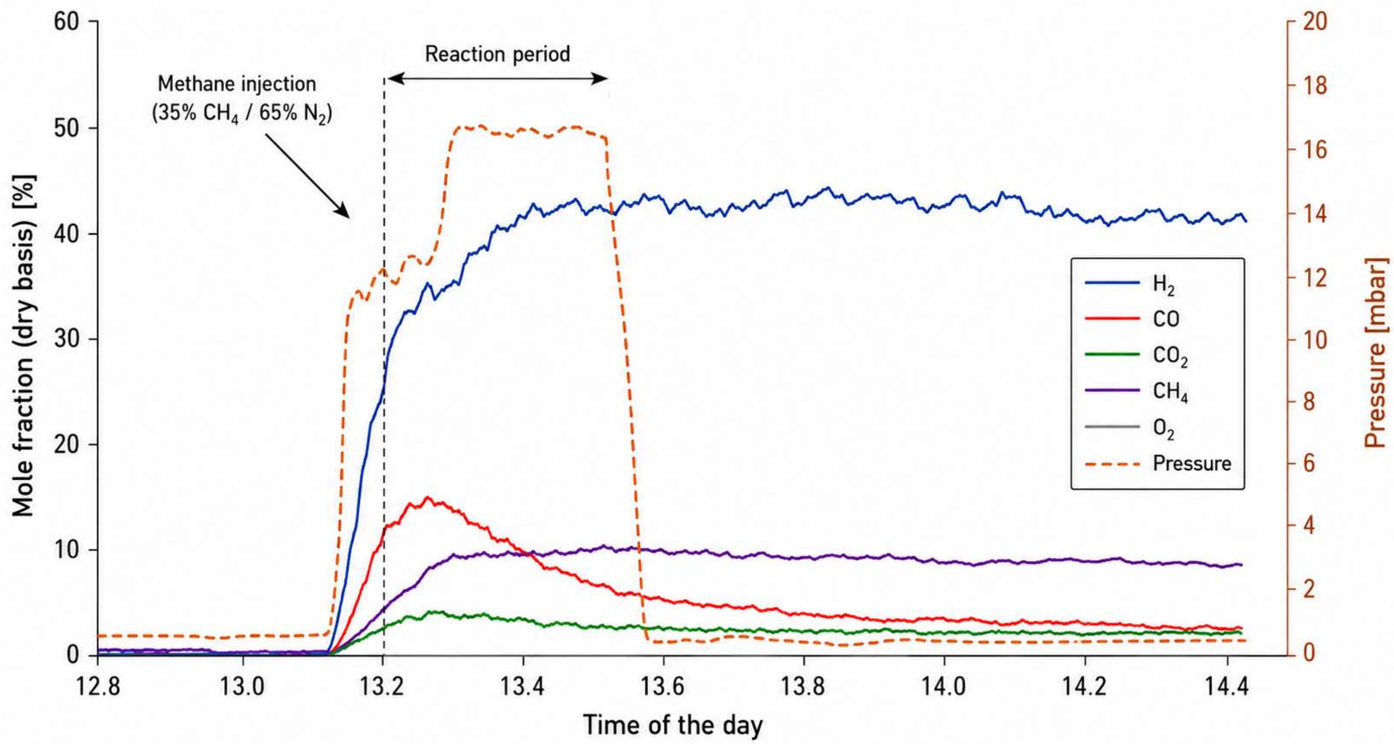

NEXT STEPS

- Improve receiver materials to withstand extreme thermal gradients and temperatures.
- Optimize reactor geometry to achieve more uniform solar heating.
- Reduce methane slip by improving gas–solid contact and residence time.
- Validate the numerical model under a wider range of operating conditions.
- Investigate strategies to minimize carbon deposition on the oxygen carrier.

Future Activities

- Develop advanced solar receivers using high-temperature alloys or ceramic composites.
- Integrate secondary concentrators (CPCs) for homogeneous heat distribution.
- Test alternative oxygen carriers with higher redox stability and oxygen transport capacity.
- Perform long-term cyclic experiments to evaluate material durability and reactor reliability.
- Scale up the reactor concept toward pilot-scale Concentrated Solar Power (CSP) applications.
- Couple the process with H_2O/CO_2 splitting to enable continuous renewable syngas production.
- Optimize operating parameters (temperature, CH_4 concentration, flow rate, pressure) to maximize H_2 yield and methane conversion.
- Extend the multiphysics model to include fluid dynamics, heat transfer, and reaction kinetics for full reactor optimization.

Politecnico di Torino

ENERGY CENTER

unite! University Network for Innovation, Technology and Engineering

CONCLUSIONS

Concentrated Solar Power (CSP)

- Demonstrated the versatility of a **parabolic dish solar concentrator** as a high-temperature renewable energy platform.

Stirling Engine

- Demonstrated the feasibility of integrating a parabolic dish solar concentrator with a Stirling engine, achieving approximately **1 kWe** of electrical power through validated thermodynamic and numerical models

ORC Polygeneration

- Demonstrated that CSP-driven ORC systems, particularly with **acetone** as the working fluid, can efficiently convert solar heat into **electricity and useful thermal energy**, enhancing overall energy utilization.

Solar Chemical Looping

- Successfully demonstrated **methane-assisted iron oxide chemical looping** under real solar conditions, producing **H_2-rich syngas (up to ~45% H_2)** while identifying receiver material durability as the main challenge for future scale-up.

REFERENCES

- M. Falchetta T. Crescenzi. *Opportunità di applicazione delle tecnologie solari termodinamiche in italia. ENEA.* 2016
- J. R. Scheffe R. J. Carrillo. "Advances and trends in redox materials for solar thermochemical fuel production". In: Solar Energy 156 (2017). Advances in Solar Thermochemistry, pp. 3–20. DOI: https://doi.org/10.1016/j.solener.2017.05.032.
- C. Perkins and A. W. Weimer. "Likely near-term solar-thermal water splitting technologies". In: International Journal of Hydrogen Energy 29.15 (2004), pp. 1587–1599. DOI: https://doi.org/10.1016/j.ijhydene.2004.02.019.
- M. Najera et al. "Carbon capture and utilization via chemical looping dry reforming". In: Chemical Engineering Research and Design 89.9 (2011), pp. 1533–1543. DOI: https://doi.org/10.1016/j.cherd.2010.12.017.
- K. Lovegrove and J. Pye, "Fundamental principles of concentrating solar power systems," in Concentrating Solar Power Technology, Elsevier, 2021
- L. Borghero et al., (2022). Methane-Assisted Iron Oxides Chemical Looping in a Solar Concentrator: A Real Case Study. Catalysts 2022, 12(11), 1477; https://doi.org/10.3390/catal12111477.
- Laporte-Azcué et al., "Material Selection for Solar Central Receiver Tubes." In: Solar Energy Materials and Solar Cells 231 (2021), pp. 111317. https://doi.org/10.1016/j.solmat.2021.111317.
- «special metals alloy 625». Disponibile su: https://www.specialmetals.com/documents/technical-bulletins/inconel/inconel-alloy-625.pdf
- «special metals incoloy 800H».Disponibile su: https://www.specialmetals.com/documents/technical-bulletins/incoloy/incoloy-alloy-800h-800ht.pdf
- «Haynes 230 properties».Disponibile su: https://www.haynesintl.com/docs/default-source/pdfs/new-alloy-brochures/high-temperature-alloys/brochures/230-brochure.pd
- «Inconel 740H properties».Disponibile su: https://www.specialmetals.com/documents/technical-bulletins/inconel/inconel-alloy-740h.pdf
- «Alloy 316H Stainless Steel Plate».
- Du, Wang, e Shen, "Thermal and Structural Evaluation of Composite Solar Receiver Tubes for Gen3 Concentrated Solar Power Systems." In: Renewable Energy 189 (2022), pp. 117-128. https://doi.org/10.1016/j.renene.2022.02.118.
- Perrero et al. (2023) https://doi.org/10.3390/en16196870

This project was funded through the Seed Fund Initiative of the European University Alliance Unite!, University Network for Innovation, Technology and Engineering. Views and opinions expressed are however those of the author(s) only and do not necessarily reflect those of the Unite! Alliance.